ISBN: 978-3-95450-214-1 ISSN: 2673-5490 doi:10.18429/JACoW-IPAC2021-MOPAB370

X-BAND RF SPIRAL LOAD OPTIMIZATION FOR ADDITIVE MANUFACTURING MASS PRODUCTION

H. Bursali[†,1], N. Catalan-Lasheras, R. L. Gerard, A. Grudiev, O. Gumenyuk
P. Morales Sanchez, B. Riffaud, CERN, Geneva, Switzerland
J. Sauza-Bedolla, University of Lancaster, UK
[1]also at Sapienza University of Rome, Italy

Abstract

The CLIC main linac uses X-band traveling-wave normal conducting accelerating structures. The RF power not used for beam acceleration nor dissipated in the resistive wall is absorbed in two high power RF loads that should be as compact as possible to minimize the total footprint of the machine. In recent years, CERN has designed, fabricated and successfully tested several loads produced by additive manufacturing. With the current design, only one load can be produced in the 3D printing machine at a time. The aim of this study is optimizing the internal cross-section of loads in order to create a stackable design to increase the number of produced parts per manufacturing cycle and thus decrease the unit price. This paper presents the new design with an optimization of the internal vacuum part of the so-called RF spiral load. In this case, RF and mechanical designs were carried out in parallel. The new cross section has showed good RF reflection reaching less than -30 dB in simulations. The final load is now ready to be manufactured and high-power tested. This new load will not only provide cost saving but also faster manufacturing for mass production.

INTRODUCTION

The CLIC main linac consists of constant gradient traveling wave, normal conducting accelerating structures and operates at X-Band (11.9942 GHz) using the $TM_{01\text{-}2\pi/3}$ mode. These traveling wave type structures require RF loads to absorb the remaining RF power after the acceleration of the electron beam. Due to the compact design of X-Band structures and the RF network of the CLIC module, limited space is available for RF loads.

In previous years, a new concept of spiral load was manufactured and tested successfully at CERN [1]. The loads were produced by additive manufacturing out of titanium. However, the current design allows for only one load during an additive manufacturing cycle as the load needs to be printed at 45° and uses supports to avoid horizontal segments, that need to be removed after manufacturing (see Fig. 1).

We decided to re-design the spiral load by an iterative process between the mechanical model and the electromagnetic simulations. This study describes the design and optimization process of the new spiral load which included three main steps; the creation and optimization of a straight waveguide parametric model, a mechanical spiral model based on this and the subsequent modifications needed to re-optimise the RF performance, and the final mechanical 3D model and manufacturing drawings.

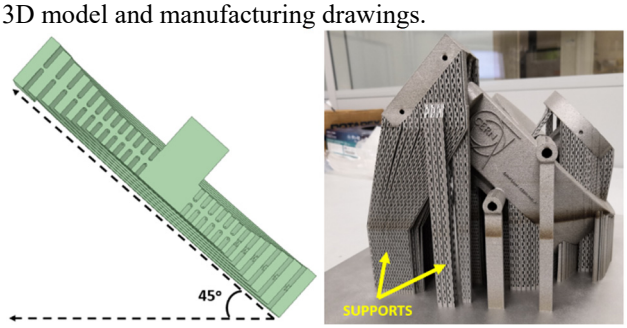

Figure 1: Spiral load vacuum model placing view (left) and load with supports after manufacturing (right).

RF LOAD STRAIGHT MODEL

The first step of the RF design started with creating a parametric straight vacuum model in CATIA [2] that was later imported into HFSS [3]. In this model, the '***b***' sides of a simple waveguide have been converted into triangular shapes, with an angle of 90° to avoid horizontal lines while printing (see Fig. 2).

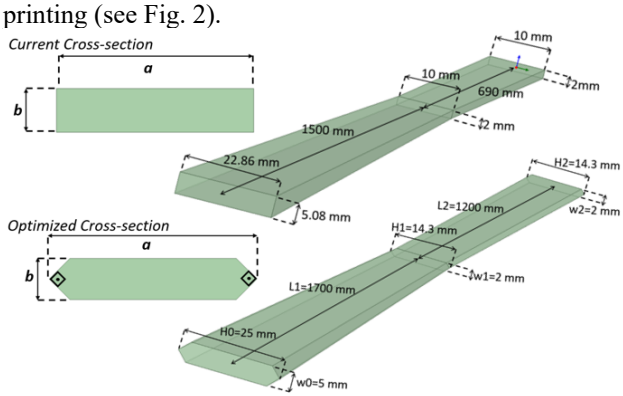

Figure 2: Current (top) and optimized (bottom) cross-section (without transition part).

The straight model is composed of three longitudinal sections; a transition from WR90 input flange to the hexagonal cross section, a slow tapering and a final straight section (see Fig. 3).

The original spiral load parameters were directly applied to the model with the new cross-section [4]. The working principle of this RF load is based on absorbing the electromagnetic signals on lossy inner waveguides, so-called 'conductor loss' [5]. We applied a finite conductivity boundary condition (6.10^5 S/m for Ti6Al4V alloy [6]) to all outer surfaces. The straight model parameters were fixed after obtaining an appropriate electric field (see Fig. 4)

† hikmet.bursali@cern.ch

ISBN: 978-3-95450-214-1 ISSN: 2673-5490 doi:10.18429/JACoW-IPAC2021-MOPAB370

distribution and reflection below -30 dB at 12 GHz (see Fig. 5) after several interactions.

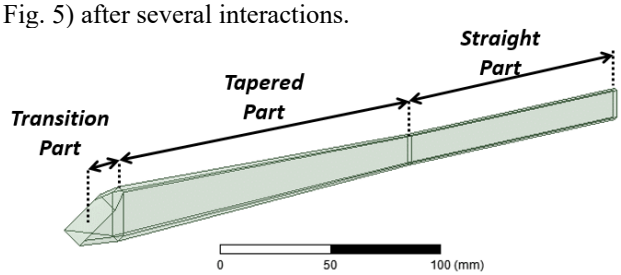

Figure 3: Straight model with longitudinal sections.

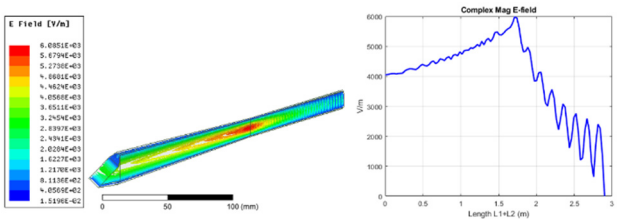

Figure 4: Electric Field (complex magnitude) Distribution along straight model.

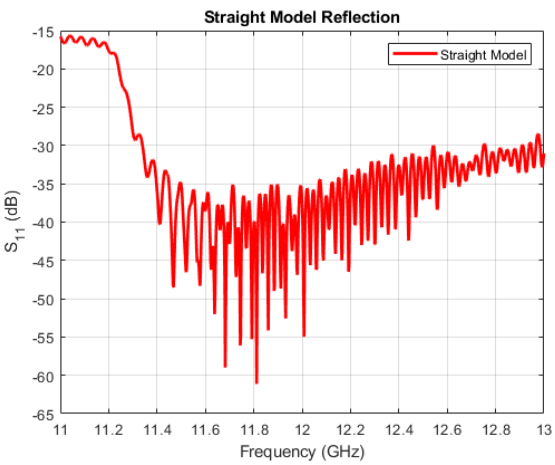

Figure 5: Straight model reflection.

RF LOAD SPIRAL MODEL

After fixing the basic dimensions of the straight load model, a CATIA spiral model (see Fig. 6) was created as an Archimedes spiral geometry [7] (see Fig. 7) on the straight part, while with keeping constant the gap between spiral surfaces on tapered part. The radius r of curvature and the pitch s, depend on the angle φ, (radius increment with increasing angle by one turn). The quantity g is the gap distance between spiral surfaces that has been adjusted to have an adequate wall. Equation (1) converts into Eq. (4) to adapt to the changing cross-section widths when reaching the tapered part where N is a real number.

$$r(\varphi) = r_0 + s(\varphi) \quad (1)$$

$$s = [M_1 M] \quad (2)$$

$$s(\varphi) = \frac{1}{2}(w(\varphi) + w(\varphi + 1)) + g \quad (3)$$

$$r(\varphi) = r_0 + (w_1 + g)\varphi + \frac{1}{2N}(w_2 - w_1)\varphi^2 \quad (4)$$

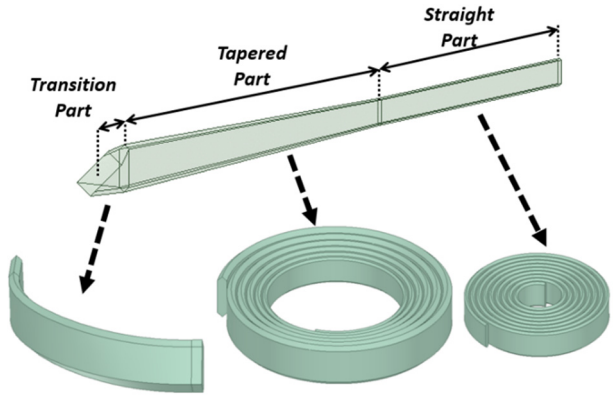

Figure 6: Spiral model creation from straight design.

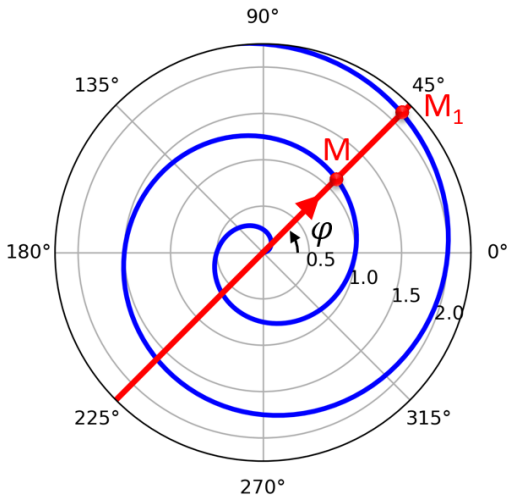

Figure 7: Archimedes Spiral Geometry.

Again, electromagnetic simulations were performed to optimize the final load RF performance. The spiral model showed reflection under -30 dB at 12 GHz close to the straight model after simulations (see Fig. 8).

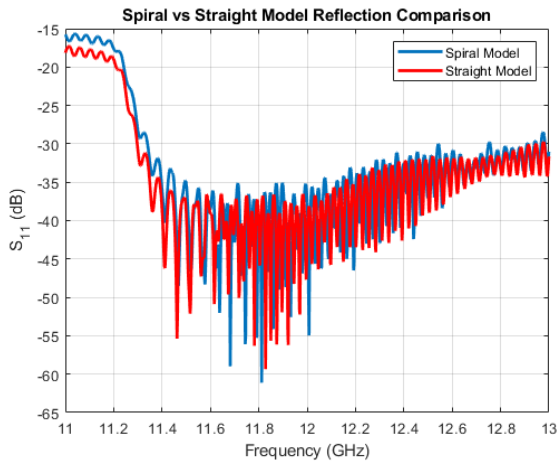

Figure 8: Reflections of Straight and Spiral Model.

ISBN: 978-3-95450-214-1 ISSN: 2673-5490 doi:10.18429/JACoW-IPAC2021-MOPAB370

PUMPING INTEGRATION & MECHANICAL DESIGN

The next step of the design process was implementing the vacuum holes between the load waveguide surfaces to provide homogenous vacuum distribution during operation. After this step, the cut-off frequency of the load shifted approximately by 350 MHz because of the decrease on the effective width of the waveguide which determines the TE_{10} mode frequency inside a rectangular waveguide (see Eq. 5 [8] where μ and ϵ describe permeability and permittivity of the signal propagation medium). This is shown in black in Fig. 9.

$$f_{c_{10}} = \frac{1}{2a\sqrt{\mu\epsilon}} \quad (5)$$

To compensate for this cut-off frequency shift we increased by 0.3 mm the H2 parameter which is the width of the waveguide at the transition between tapered and straight part (see Fig. 10).

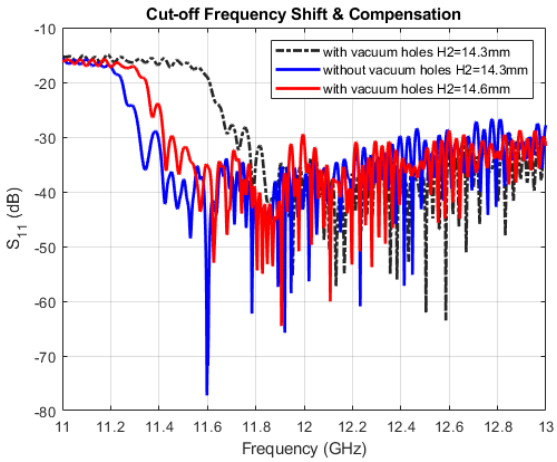

Figure 9: Cut-off frequency shift and signal peak on reflections with and without vacuum pumping holes and after correction of the waveguide dimensions.

After compensating the frequency shift, we observed an increase on reflection at 12 GHz as shown in red in Fig. 9. This is caused by the asymmetry on the last turn of the spiral which only has vacuum holes in one side.

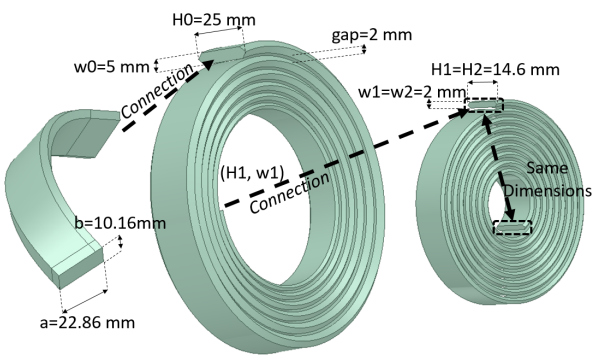

Figure 10: Spiral model parameters and dimensions.

A tuning hole with a 3 mm diameter was placed under the transition part to reduce the reflection at 12 GHz. As a last step, we performed RF simulations with an average Ti6Al4V alloy roughness, 50 µm [9]. The final reflection is expected to be below -30 dB at 12 GHz (see Fig. 11).

The mechanical design has been completed by integrating cooling channels and a CF16 vacuum flange to the middle part of the model (see Fig. 12).

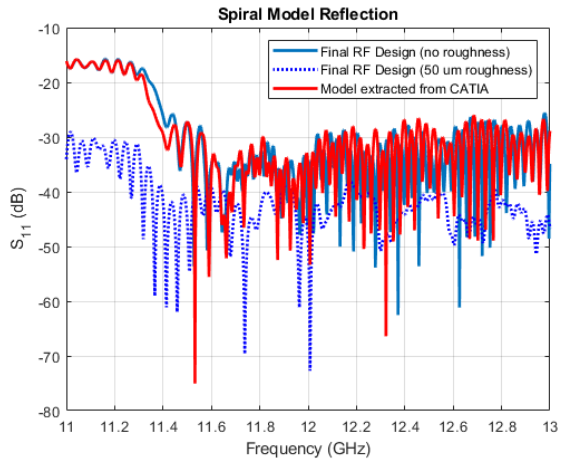

Figure 11: Reflection of final RF design (with and without roughness) and vacuum model extracted from CATIA.

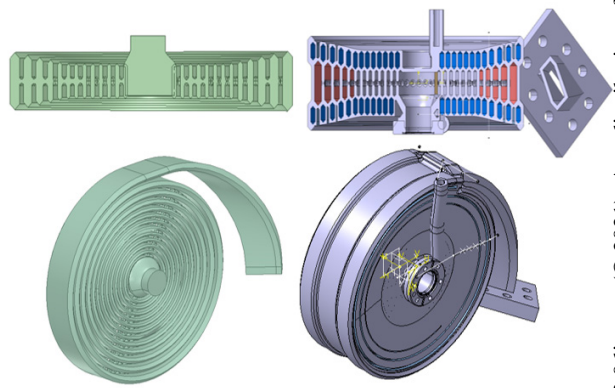

Figure 12: RF (left) and Mechanical (right) Design cross-sectional and full model views.

CONCLUSION AND FUTURE WORK

By using parametric models both in CATIA and in HFSS, the cross-sectional optimization of a new X-Band RF spiral load has been completed as RF and mechanical design. This new design will provide cost savings by allowing the horizontal placement inside the 3D printing machine and the stacking of several units. The production of the first prototype is imminent and will be followed by low and high-power RF tests.

REFERENCES

[1] N. Catalan-Lasheras *et al.*, "High Power Conditioning of X-Band RF Components", in *Proc. 9th Int. Particle Accelerator Conf. (IPAC'18)*, Vancouver, Canada, Apr.-May 2018, pp. 2545-2548. doi:10.18429/JACoW-IPAC2018-WEPMF074

[2] CATIA, https://www.3ds.com/

ISBN: 978-3-95450-214-1 ISSN: 2673-5490 doi:10.18429/JACoW-IPAC2021-MOPAB370

[3] HFSS, https://www.ansys.com/

[4] G. L. D'Alessandro, "Development of X-Band High Power RF Load for CLIC Applications Using Additive Manufacturing Techniques", BSc. thesis, CERN, Geneva, Switzerland, 2015.

[5] D. M. Pozar, "Transmission Lines and Waveguides", in *Microwave Engineering*, 4th Ed. New York, NY, USA: Wiley, 2011, pp. 97.

[6] Zhu Ke *et al.*, "Measurement of Electrical Conductivity of Porous Titanium and Ti6Al4V Prepared by the Powder Metallurgy Method", *Chinese Phys. Lett.*, vol. 24, pp. 187-190, 2007. doi:10.1088/0256-307X/24/1/051

[7] E. Lockwood, "Spirals", in *Book of Curves,* Cambridge, UK: Cambridge University Press, 1961, pp. 173-176.

[8] D. M. Pozar, "Transmission Lines and Waveguides", in *Microwave Engineering*, 4th Ed. New York, NY, USA: Wiley, 2011, pp. 113.

[9] N. M. Heretis, P. Spanoudakis, and N. Tsourveloudis, ''Surface Roughness characteristics of Ti6Al4V alloy in conventional lathe and mill machining'', *International Journal of Surface Science and Engineering (IJSURFSE),* vol. 3, no. 5/6, pp.435-477, 2009. doi:10.1504/IJSURFSE.2009.029139